Bio-inspired dual-anchor burrowing: effect of vertical curvature of the shell

Huang, S., S.M.[1] and Tao, J., A.M.[2]

[1]PhD Student, Center for Bio-mediated and Bio-inspired Geotechnics (CBBG), Arizona State University, Tempe, AZ. Email: shuang64@asu.edu

[2]Associate Professor, Center for Bio-mediated and Bio-inspired Geotechnics (CBBG), Arizona State University, Tempe, AZ. Email: julian.tao@asu.edu

ABSTRACT

Many organisms rely on dual-anchor strategy to burrow. A prominent biological role model is the Atlantic razor clam. By concerting the shape changing of various body parts: opening/closing of a rigid shell, extension/contraction of the muscular foot, and inflation/relief of the distal pedal, razor clams can burrow very effectively and efficiently. Using 3D Discrete Element Method modeling, the interactions between two clam inspired dual-anchor penetrators and the surrounding granular media were captured at multiscale. A penetrator includes two major parts: a slender "shell" with time-varying diameter, and a conical "foot". Two different penetrators were considered: one with a uniform cylindrical shell and the other with a fusiform shell. The granular material consists of spherical particles with an upscaled particle size distribution of Ottawa F65. Microscale parameters are calibrated and validated with experimental triaxial test data. The impact of shell morphology is studied. It is found that opening of the shells compresses the soil around the shell to form anchorage, and at the same time releases the stress around the foot. A fusiform shell morphology is found to have limited influence on the penetration resistance and the shell anchorage during the foot penetration process. A systematic parametric study is still needed to test the hypothesis that a streamlined shell improves the burrowing performance of razor clams.

Keywords: razor clam, dual-anchor, burrowing, curvature

INTRODUCTION

Many organisms in nature locomote through the substrate by changing shape of their bodies. Examples include: the earthworm cyclically alternate the expansion and extension of the front tip to gain the anchorage and thrust for the underground advancement (Ruiz et al. 2015); the polychaete *Cirriformia tentaculate* cyclically expands the anterior body part to crack the soil ahead and advance the body (Dorgan 2015). These organisms adopt a similar burrowing strategy, which is termed a dual-anchor strategy. By alternatively changing shape of different body parts, the organisms obtain the anchor and thrust required for the advancement into the substrate.

The Atlantic razor clam (*Ensis directus*) represents a prominent model among the dual-anchor burrowers in nature, because of its exceptional burrowing performance realized through a simple body structure and simple control strategy. The subsurface burrowing of razor clam simply relies on a simple body structure: a slender rigid shell and an internal hydraulic system to control the cyclic expansion/contraction of the mantle cavity as well as protrusion/contraction of a tubular muscular foot. In general, the shell opens and compresses the surrounding soil, forming a penetration anchor for the probing and extension of foot; then the razor clam closes the shell, pushes the body liquid into and dilates the foot, creating a terminal anchor for the pulling down of the shell into the substrate (see Figure 1). By cyclically alternating the penetration and terminal anchors, the razor clam can locomote underground very effectively and efficiently. The simple structure and easy control strategy inspire engineers in developing a novel subsurface self-burrowing robot, which can be widely applied to, subsurface exploration, underground wireless sensing network, contamination monitoring and *etc*.

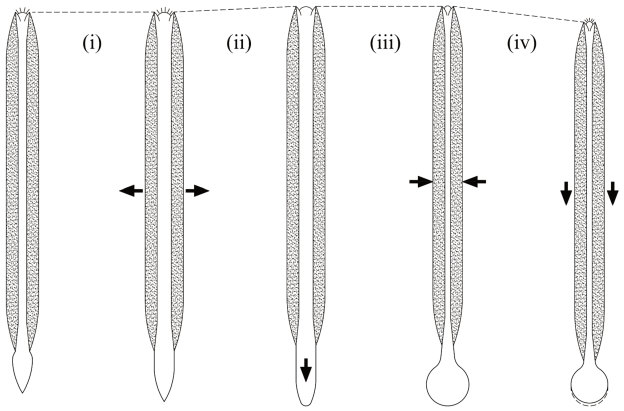

Figure 1. A typical burrowing cycle of the razor clam. The dotted line denotes the depth and arrows indicate the direction of movement of the foot and valves. (i) Opening of the shell. (ii) The foot probes downward. (iii) shell adduction pushes body fluids into the foot to form a terminal anchor. (iv) The foot retracts, pulling the shell downward, and the body returns to its initial shape (Trueman 1967).

Previous studies attributed the high burrowing efficiency of razor clams to the local fluidization caused by the closing and uplifting of the shell (Winter et al. 2014). The local fluidization was elegantly explained by combining the soil mechanics and fluid mechanics, and a robotic penetrator ('RoboClam') was designed to demonstrate its efficiency (Jung et al. 2011; Winter et al. 2014). Nevertheless, the importance of other steps is not sufficiently explored. Huang and Tao (2018) found an interplay exist between the shell-opening and foot penetration when modelling a clam-inspired two-body penetrator (a cylindrical 'shell' and a conical 'foot') burrowing into a synthetic dry sand. The shell-opening process not only creates a penetration anchor, but also causes a stress relief in the soil around the foot, which results in the penetration resistance reduction; meanwhile, the foot penetration tends to weaken the penetration anchorage by dilating the soil around the opened shell.

To obtain a net advancement effectively and efficiently in a burrowing cycle using dual-anchor strategy, it requires to generate firm anchors, to minimize the 'slip' and to minimize the burrowing resistance. Many bivalve clams enhance the penetration anchor by evolving a rough shell surface and reduce the penetration resistance by rocking their body (Germann et al. 2010; Stanley 1975).The rough shell surface enhances the ability of gripping the surrounding soil during shell-opening but resist the pulling-down of the shell (Stanley 1975; Trueman et al. 1966). This in a sense explains why many rounded bivalves are shallow and slow burrowers. The *Ensis* species are rapid burrowers and tend to have a slender shell with smooth surface and penetrate into soil without rocking (Stanley 1970). The slenderness of the shell increases the interaction area between the shell and the surrounding soil, which facilitates in forming a firm anchor but increases the resistive force to pull down the shell. It is well known that many animals use fusiform streamlined body shape to reduce the fluid drag to achieve effective locomotion in air and water (Lighthill 1960; Swaddle and Lockwood 2003). It is also interesting to observe that the projection profile from the ventral to dorsal of a razor clam shell is a fusiform. The digging behavior of a razor clam happens in a low-Reynolds quasi-static granular flow environment (Hosoi and Goldman 2015). It is then assumed that the shell shape may also play an important role in the burrowing cycle.

This study used the DEM modelling technique to explore the role of shell shape in a typical burrowing cycle in the dry sands. The penetrator was simplified as a two-body structure, with an expandable slender 'shell' and a protrusible conical 'foot'. As a preliminary trial, only two shell shapes are considered.

METHODOLOGY

Numerical Method. *PFC 3D 5.0,* a commercial software developed by ITASCA (Itasca Consulting Group 2015), was utilized for the DEM modelling. The model is composed of discrete rigid spherical particles. The built-in linear elastoplastic contact law with rolling resistance considered is implemented to describe the interactions between the contacting entities, for simplicity and to reduce computation burden. The particle shape effect was accounted for by considering the rolling resistance between any two contacting particles. The rolling resistance to rotation is linearly related to the accumulated relative rotation of the two contacting particles at the contact point. A rolling resistance ratio μ_r was introduced and combined with the real-time normal contact force and the radius of the contacting particles. For details about the rolling resistance model, please refer to (Itasca Consulting Group 2015). No cohesion was considered in this study. Meanwhile, a non-viscous damping strategy was used during sample preparation (Cundall 1987) to facilitate a rapid convergence to a quasi-static state. The local damping was removed when the sample preparation was completed.

Calibration and Validation. Within the DEM framework described above, four material parameters are required to calibrate: the normal contact modulus and stiffness ratio of the material, interparticle friction angle, and the interparticle rolling resistance coefficient. A cuboid DEM

specimen with specific porosity was generated using the radius expansion method. The sample had a size of 6mm × 3mm×3mm and contains 8,498 particles within rigid wall boundaries. The particle size distribution of the DEM sample generally reproduced the feature of the Ottawa F65 with the fine part truncated (see Figure 3b). The servo control mechanism was implemented to control the sample confining condition during the test. The experimental results of drained triaxial compression tests from (Badanagki 2019) were utilized for calibration and validation. Through trial-and-error, a set of parameters was determined and provided the best fit to the experimental results, as shown in Figure 2. In general, the numerical sample built with the calibrated parameters was found to have a comparable shear strength with the experimental results, but a slightly higher Young's modulus and a smaller dilation angle than the Ottawa F65 used in the physical experiments. The determined parameters are included in Table 1.

Table 1 Parameters for the contact law

Parameters	Unit	Value
Normal contact modulus, E	Pa	2.0e8
Stiffness ratio, α	\	0.2
Interparticle friction angle, ϕ	°	27
Interparticle rolling resistance coefficient, μ_r	\	0.7

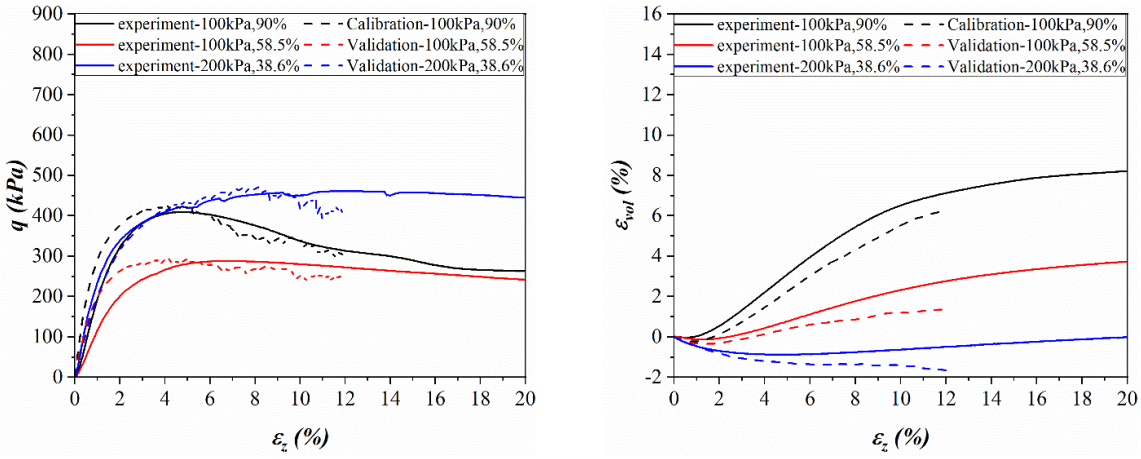

Figure 2. DEM parameter calibration and validation. (a) deviator stress vs. axial strain (b) volumetric strain vs. axial strain

Model Construction. The objective of the current study is to explore the role of shell shape in a burrowing cycle. The burrowing performance is a result of combined effects from different factors, such as the burrowing kinematics, shapes of various body parts, soil conditions and *etc*. Using a realistic and complex model can offer the best reproduction of the real behavior, but inevitably causes an extremely high computation burden. It is also challenging to identify and clearly understand the role of a specific aspect in the burrowing cycle from a complex model. Therefore, appropriate simplifications are necessary in the simulation in order to highlight the function of

shell shape in the dynamic burrowing process with acceptable accuracy. As a result, a DEM sample containing 343,125 particles (see Figure 3a) was generated within a closed cylindrical chamber. The particle size distribution of Ottawa sand F65 was uniformly scaled up by 25 times and the finer part is truncated, as shown in Figure 3b. The interparticle friction angle was set as zero at the radius expansion process; the sample was cycled till the average contact force is small enough (10^{-10} N). After that, the particles were freely deposited under gravity effect and the sample porosity was adjusted by manipulating the interparticle friction angle. The interparticle friction angle was set back to 27° when the targeted sample porosity was achieved and the sample was further cycled to the quasi-static equilibrium state.

The penetrator was simplified as a two-body structure: an expandable fusiform 'shell' and a protrusible conical 'foot'. Based on the measurements of the projection profile from the ventral to the dorsal side of a real juvenile clam shell, the thickness difference between the middle and both ends of the shell is about 2 mm, and the longitudinal curvature of the shell can be roughly fitted using an elliptical curve. In such a case, the fusiform 'shell' was considered as a slender spheroid (or, prolate) with both ends truncated. At the bottom end of the shell, the cross section shares a same diameter with the top surface of the conical 'foot'. Opening of the 'shell' is achieved by uniformly increasing the radius of each circular cross section of the truncated spheroid with a user-defined rate, which is 0.01m/s in this study. Also, a uniform cylindrical 'shell' is considered as a control for comparison, details about the dimension of the penetrators can be find in Figure 3c and Table 2. Note that, neither of the chosen shapes represents the realistic shape of the razor clam shells. In fact, the cross-sections of razor clam shells are not circular, but also fusiform. In this study, to isolate the effect from the vertical curvature, the cross-sectional area of the shell was taken as circular. These treatments resulted in a larger total body volume (94 cm^3) in Case #2 than that in Case #1 (77 cm^3).

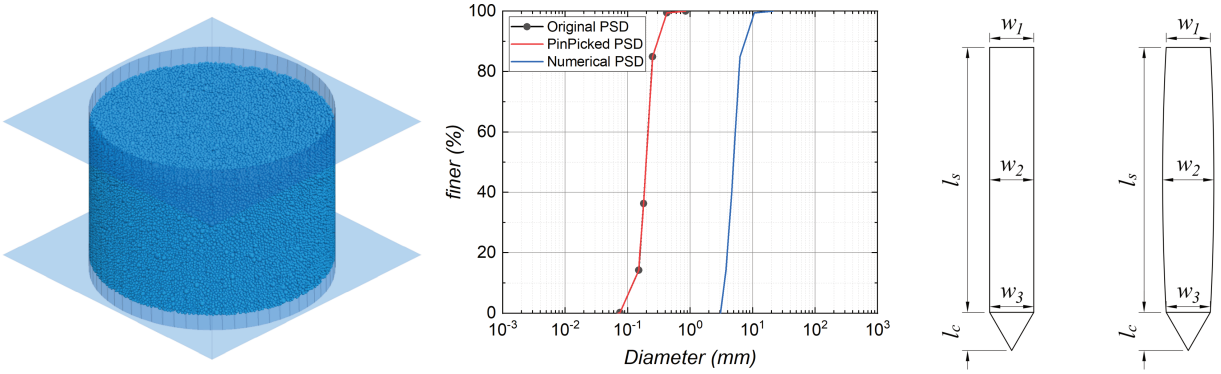

Figure 3. (a)Numerical sample (b)Particle size distribution (c)Penetrator profile

Table 2 Shell longitudinal curvature parameters

Case #	w_1 (mm)	w_2 (mm)	w_3 (mm)	l_s (mm)	l_c (mm)	Form
Case #1	25	25	25	150	21.65	cylinder
Case #2	25	29	25	150	21.65	fusiform

Different shell shapes may directly affect both the shell opening stage and shell retraction stage; the foot penetration stage may also be affected indirectly. In order to exclude the potential interplay between the shell opening and shell retraction, the shell shape effect on the shell retraction and the shell-opening stages were explored independently: 1) To study the penetration resistance, the penetrator is generated along the chamber central axis as the tip situates at the top surface of the sample; and the penetrator is then directly penetrated into the sample without shell opening; and 2) to study the anchorage formation, the penetrator is generated within the sample along the chamber central axis; and opening and uplifting of the shell is activated in sequence. Details on the simulation cases and penetrator kinematics are summarized in Table 3.

Table 3 Simulation summary

Model Set ID	Initial sample porosity	Initial Penetrator Location	Penetrator Kinematics	Kinematic Characteristics	Shell Shape
1	0.412	Above the sample surface	Direct penetration	v_p = 1cm/s, t_p = 15s	Case #1, Case #2.
2	0.412	Below the sample surface	Shell-opening; Shell-uplifting	v_{exp} = 1cm/s, t_{exp} =0.25s; v_{uplift} = 1cm/s, t_{uplift} =0.2s;	Case #1, Case #2

v_p: penetration rate, t_p: duration of penetration; v_{exp}: shell radius increasing rate, t_{exp}: duration of shell-opening; v_{uplift}: shell uplifting rate, t_{uplift}: duration of shell uplifting

Characterizations of the Simulation Process. Several parameters are defined below to aid in discerning the DEM simulation results.

1. *Tip resistance.* The tip resistance q_c is defined as the net vertical pressure applied on the conical foot;

2. Shell resistive force. The shell resistive force F_a is defined as the summation of the vertical component of all the contact forces applied on the shelled body;

3. *Expansion resistive force.* The expansion resistive force F_{rad} is defined as the mathematic summation of the normal component of all the contact forces applied on the 'shell'.

RESULTS AND DISCUSSIONS

Macroscale Results. The tip resistance and the shell resistive force during direct penetration simulation were monitored, as shown in Figure 4. In general, the tip resistance increases with increasing travel distance into the soil (see Figure 4a). The data is quite noisy and contains obvious oscillations, which is mainly caused by the limited foot-and-particle contact number (Butlanska et al. 2010) and can be filtered out. A second order polynomial function is utilized to extract the steady resistance data from the raw tip resistance curves for both cases (see Figure 4a). Both the fitting curves are with a R^2 of 95% and included in Figure 4b for comparison. The penetrator with a cylindrical 'shell' (Case #1) experienced a lower resistance than the penetrator with a fusiform 'shell' (Case #2) during the direct penetration process. Since fusiform shape is normally considered more "streamlined" than cylindrical shape, it was expected that the shell resistive force

in case #2 should be lower than that in Case #1. However, as shown in Figure 4c, that is not the case and the shell resistive forces for the two cases are similar (see Figure 4c).

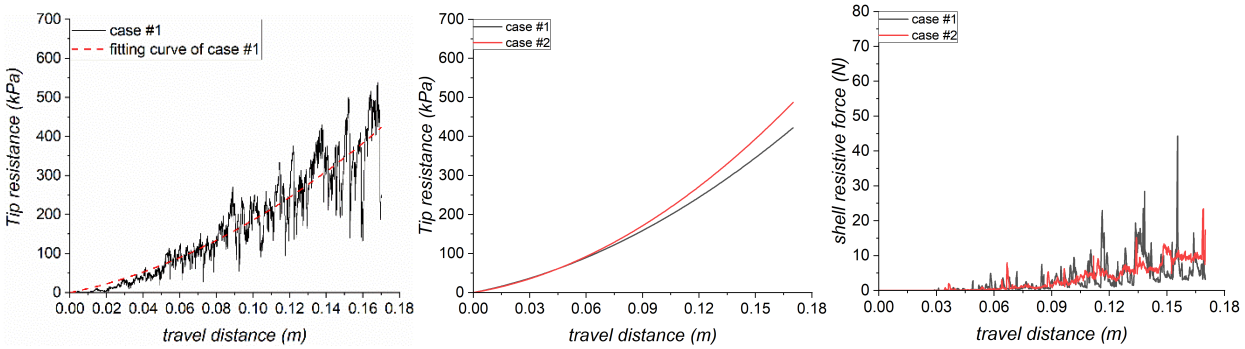

Figure 4. Tip resistance and shell reistive force during direct penetration simulation. (a) tip resistance during direct penetration for case #1 (b) poly-fitted tip resistance for both cases (c) shell resistive force during direct penetration for both cases.

To examine the shape effect on anchorage formation, the expansion resistive force during shell-opening and the shell resistive force during shell uplifting for both cases were monitored and included in Figure 5. It is observed that a fusiform 'shell' results in a comparable F_{rad} with cylindrcal-shell penetrator when the 'shell' diameter increment ratio is smaller than 12%; However, the F_{rad} of Case #2 becomes higher than Case #1 when the diameter increment ratio is beyond 12% (see Figure 5a). Before expansion, the tip resistive force in Case #1 and Case #2 is 36 N and 37 N, respectively; after expansion, the tip resistive force for the two cases is found to be 0.6 N and 0.2 N. It is clear that shell expansion has a significant effect on reduction of the tip resitive force, which will facilitate an easier repenetration in the subsequent burrowing cyce as found in previous numerical studies (Huang and Tao 2018). It also shows that with a higher cost to expand, Case #2 resulted in a higher benefit as well, that is, a more significant tip resitive force reduction.

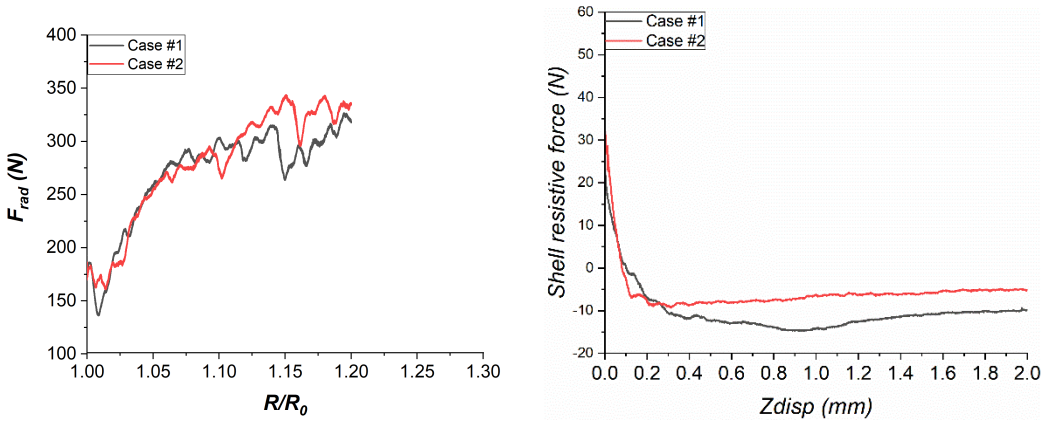

Figure 5. (a) Expansion resistive force during shell-opening (b) Shell resistive force during shell-uplifting.

The appearance of a negative shell resistive force indicates the formation of penetration anchor during shell-uplifting. The lower the shell resistive force becomes, the stronger and firmer the penetration anchor is. As shown in Figure 5b, by uplifting the opened shell slightly, the shell resistive force rapidly decreases for the first 0.3 mm, and turns into a negative stable value thereafter. In addition, the fusiform 'shell' tends to form the penetrator anchor faster than the cylindrical 'shell' during shell-uplifting. However, the resulting anchorage of the fusiform 'shell' is lower than that of the cylindrical 'shell', as indicated in Figure 5b. With a more streamlined body, Case #2 resulted in a lower anchorage, which was not initially expected, and inconsistant with the effect on penetration (Figure 4). This observation highlights the dependence of the shape effect on the penetration direction, which will be discussed further in the following sections.

Microscale Analysis. To illustrate the particle response corresponding to the kinematics of the penetrator with different shell shapes, the displacement field for particles are extracted. A binary criterion is used for visualization. Particles displaced upward are colored in black, otherwise in light grey. Figure 6 presents the obtained binary particle displacement field created by two penetrators by the end of direct penetration (6a and 6b) and by the end of shell-opening (6c and 6d).

As shown in Figure 6a and 6b, the binary displacement fields caused by both penetrators display several common features: 1). particles closed the 'shell' are driven downward by the advancing 'shell'; 2). two boundary curves can be identified to differentiate the upward and downward displacing particles for area below the foot-shell interface level. The boundary curve originates from the foot-shell interface and extends outward and obliquely to the external boundary; 3). Particles located below the two boundary curves are displaced downward due to the advancement of the penetrator; 4). Particles above the boundary curves are displaced upwards to accommodate the increasing submerging volume of the penetrator.

Nevertheless, the profiles of the downward displacement field around the 'shell' are slightly different. The profile created by the cylindrical shell penetrator is a uniform rectangular area (see Figure 6a); whereas the profile created by the fusiform shell penetrator is a trapezoidal area, with the lower end wider than the upper end (see Figure 6b).

The binary displacement field created by the shell-opening of penetrator varies with the shell shapes, as indicated in Figure 6c and 6d. Although the similarity between the two displacement fields are small, several interesting common features can still be extracted: 1. In general, particles located in two major areas tends to move upward: 1) particles located on both sides of the 'shell' tend to move upward in order to accommodate the increased penetrator volume by shell-opening; 2) Both upward and downward displacement occur around the foot-shell interface level; and 3) Particles below the conical foot tend to move upward by the end of shell-opening. The upward displacement for particles below the foot is mainly caused by the stress relief, or unloading of the sands between the cone tip and the bottom boundary.

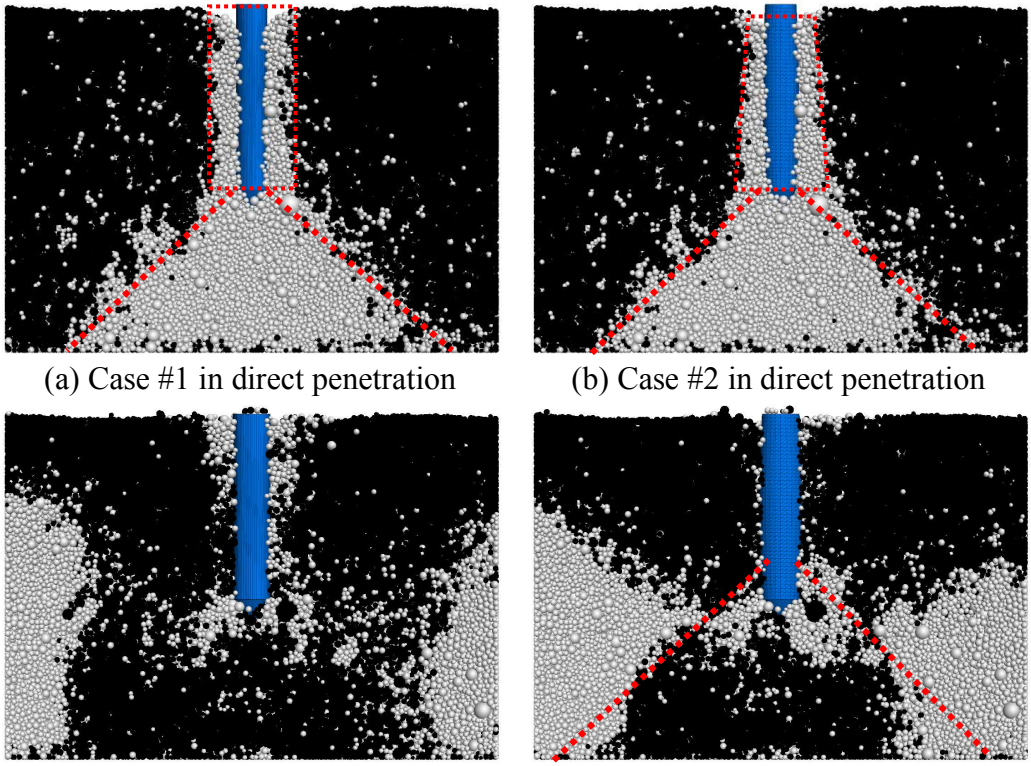

(a) Case #1 in direct penetration (b) Case #2 in direct penetration

(c) Case #1 in shell-opening (d) Case #2 in shell-opening

Figure 6. The binary particle displacement field for particles contained in a vertical section by the end of direct penetration. Black particle represents upward displacement; grey particle represents downward displacement.

Opening of the fusiform 'shell' creates a larger downward displacement zone around the foot because of the lower tapped end. In addition to pushing the particles on both sides laterally, the lower tapped surface also attempts to push the surrounding particles downward and obliquely. Also, the upward displaced particle zone below the foot seems to be constraint below two boundary curves, as indicated in Figure 6d. It is also interesting to note that particles close to the top end of the cylindrical shell penetrator are displaced downward, although the amount of downward displacing particles is small.

The force chain network presents a visualization of the load transfer across the sample. In Figure 7a and 7b, the force chain networks within the vertical section are extracted by the end of direct penetration and corresponds to the binary displacement fields in Figure 6a and 6b. In general, the distribution of strong force chains for both penetration simulations are similar and mainly concentrated around and below the foot due to the penetrating foot. In addition, the distribution pattern also follows the displacement 'boundary-curve' identified in Figure 6a and 6b. The strong force chains below the two boundary curves radiate from the cone surface and extend outward in a direction perpendicular to the cone surface; strong force chains above the boundary curves branch out from the boundary curve and extend obliquely to the external boundary (see Figure 7a and 7b). Moreover, different from the cylindrical-shell penetrator, direct penetration using a fusiform-shell

penetrator also causes strong force concentration around the lower tapped surface of the ‘shell’. This phenomenon also explains the differences in shell resistive force in Figure 4c and the closed-to-shell binary displacement profile in Figure 6a and 6b.

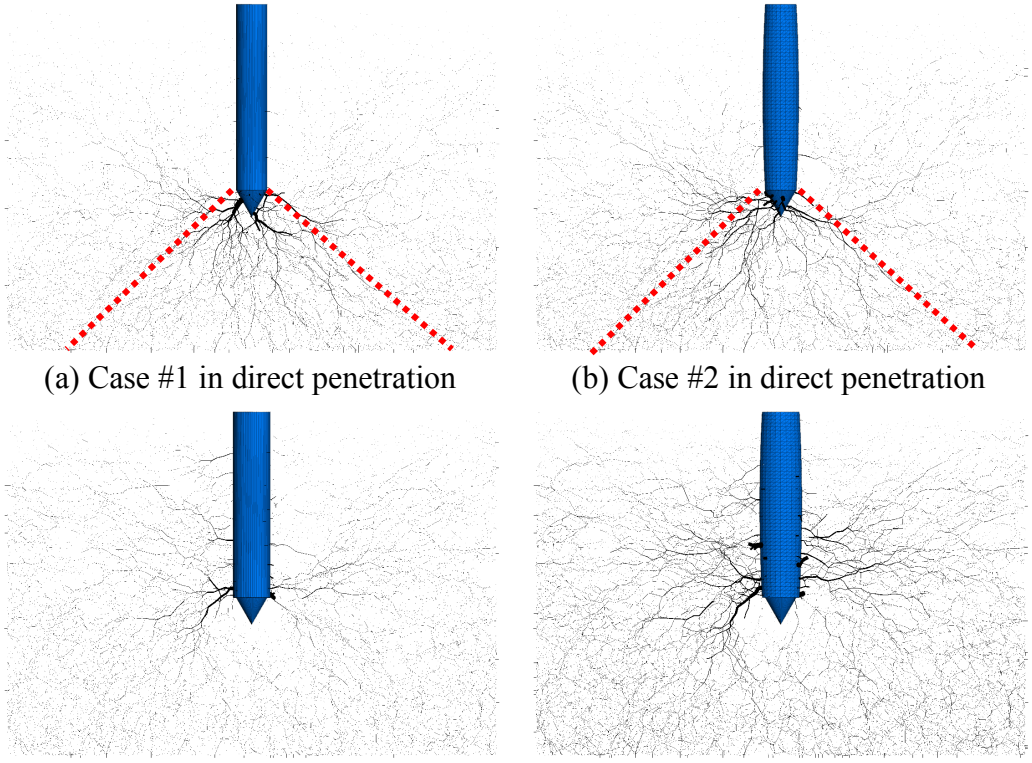

(a) Case #1 in direct penetration (b) Case #2 in direct penetration

(c) Case #1 in shell-opening (d) Case #2 in shell-opening

Figure 7. The force chain network for particles contained in a vertical section by the end of shell-opening. Only forces exceeding average normal contact force are displayed. Forces exceeding the average value +5standard deviations are illustrated in black, otherwise shown in greyscale, with the average value in light grey. Force chain thickness is linearly proportional to the force magnitude.

Figure 7c and 7d present the force chain networks at the end of the shell-opening stages. Opening of the ‘shell’ compacts the surrounding particles and generates a strong force chain around the opening shell. Meanwhile, an obvious weak force chain network can be identified around the conical ‘foot’, which indicates stress relief. It is also worthy to note that the strong force chains created by opening of the fusiform ‘shell’ mostly concentrated around and radiate from the lower tapped surface of the ‘shell’. This phenomenon is consistent with the observations in Figure 6d.

DISCUSSION AND CONCLUSION

This study utilized the discrete element method to explore the role of shell shape in the burrowing cycle. Two types of shell shapes are considered, a fusiform 'shell' and a cylindrical form 'shell'. In general, using a fusiform shell result in a higher resistive force during shell retraction (penetration) process but lower anchorage force during uplifting.

Opening of the 'shell' compacts the particles around the penetrator, which causes strong force concentration around the shell (see Figure 7c and 7d). Particles located around the level of foot-shell interface tend to be driven towards the external boundary by the interparticle frictional force. The soil behavior in this local area during shell-opening is similar to the direct shear test. The tapped surface on the fusiform 'shell' tends to enhance the particle lateral displacements effect by pushing the particles obliquely and laterally, as shown in the strong force chains concentration around the lower tapped side of the fusiform 'shell' (see Figure 7d). As a result, the local downward displacement field around the foot in Figure 6d is more obvious than Figure 6c. Also, the shell-opening creates a stress relief zone around the foot. Unloading the sand between the cone tip and the lower boundary, the particles move upward. It is then assumed that by manipulating the expansion ratio, a more significant stress relief can be created, especially in a deep, high-confinement area.

It is hypothesized that the razor clams benefit from the streamlined shell when burrowing. To have a higher burrowing efficiency, it is better to have lower penetration resistances; to have a higher burrowing effectiveness, it is better to have higher anchorage forces. A fusiform shape is normally considered as more streamlined than a uniform cylinder. However, the results from this study show that the vertical curvature itself doesn't contribute to reduction of penetration resistance nor increase of anchorage during burrowing. As an analogy, the penetration force in sand is similar to drag force in fluid flow. Drag force includes form drag, skin drag and lift-induced drag. Form drag depends on relative velocity and the longitudinal shape, i.e., more streamlined shapes leads to lower form drag; skin drag is caused by friction and depends more on the wetted surface area and the viscosity of the fluid. Lift-induced drag is less relevant to vertical penetration in sand. The effect of the longitudinal profile or vertical curvature in this study on reducing the penetration force is more pronounced when the shell is moved upward, where the soil has little confinement and free to move/flow; for downward penetration, however, the particles move very slowly; the form drag is not reduced significantly and the skin-friction drag dominates. Razor clam burrows in saturated sand and uses shell movement and water injection to fluidize soil. The fluidized soil can then be considered as a flowing fluid when the shell is retracted. Therefore, by having a streamlined body, form drag will play a more significant role during shell retraction after shell contraction and the total drag force can be greatly reduced. A major drawback of the simulation setup in this study is that shell contraction is not well represented so the penetration process is less representative of the retraction process. More systematic evaluations should be taken in order to validate or falsify the hypothesis on the effect of streamlining on burrowing performance. It is also worthy to explore, both numerically and experimentally, the effect of the shape of the cross section, the shape of the foot, as well as the dependency of shape effects upon the soil condition, and penetration direction and rate in the future work.

ACKNOWLEDGEMENT

This material is based upon work supported by the National Science Foundation (NSF) under NSF CMMI 1849674. Any opinions, findings and conclusions or recommendations expressed in this material are those of the authors and do not necessarily reflect those of the NSF.

REFERENCE

Badanagki, M., (2019). "Centrifuge Modeling of Dense Granular Columns in Layered Liquefiable Soils with Varying Stratigraphy and Overlying Structures." Ph.D. thesis, Department of Civil, Environmental, and Architectural Engineering, University of Colorado Boulder, Colorado, USA.

Butlanska, J., Arroyo, M., and Gens, A. (2010). "Size effects on a virtual calibration chamber." *Numerical methods in geotechnical engineering. CRC Press, Balkema*, 225-230.

Cundall, P. (1987). "Distinct element models of rock and soil structure." *Analytical and computational methods in engineering rock mechanics*, 129-163.

Dorgan, K. M. (2015). "The biomechanics of burrowing and boring." *J Exp Biol*, 218(Pt 2), 176-183.

Germann, D., Schatz, W., and Hotz, P. E. (2010). "Bivalve burrowing robots: correlating shell morphology and movement pattern with burrowing efficiency." *Design & Nature V: Comparing Design in Nature with Science and Engineering*, 5, 389.

Hosoi, A. E., and Goldman, D. I. (2015). "Beneath Our Feet: Strategies for Locomotion in Granular Media." *Annual Review of Fluid Mechanics, Vol 47*, S. H. Davis, and P. Moin, eds., Annual Reviews, Palo Alto, 431-453.

Huang, S., and Tao, J. (2018). "The interplay between shell opening and foot penetration of a model razor clam: Insights from DEM simulation." *B2G Atlanta 2018 Bio-mediated and Bio-inspired Geotechnics*.

Itasca Consulting Group, I. (2015). "Guide book: theory and background PFC3D."

Jung, S., Winter, A. G., and Hosoi, A. (2011). "Dynamics of digging in wet soil." *International Journal of Non-Linear Mechanics*, 46(4), 602-606.

Lighthill, M. (1960). "Note on the swimming of slender fish." *Journal of fluid Mechanics*, 9(2), 305-317.

Ruiz, S., Or, D., and Schymanski, S. J. (2015). "Soil Penetration by Earthworms and Plant Roots—Mechanical Energetics of Bioturbation of Compacted Soils." *PloS one*, 10(6), e0128914.

Stanley, S. M. (1970). *Relation of shell form to life habits of the Bivalvia (Mollusca)*, Geological Society of America.

Stanley, S. M. (1975). "Why clams have the shape they have: an experimental analysis of burrowing." *Paleobiology*, 1(1), 48-58.

Swaddle, J. P., and Lockwood, R. (2003). "Wingtip shape and flight performance in the European Starling Sturnus vulgaris." *Ibis*, 145(3), 457-464.

Trueman, E. (1967). "The dynamics of burrowing in Ensis (Bivalvia)." *Proceedings of the Royal Society of London B: Biological Sciences*, 166(1005), 459-476.

Trueman, E., Brand, A., and Davis, P. (1966). "The effect of substrate and shell shape on the burrowing of some common bivalves." *Journal of Molluscan Studies*, 37(2), 97-109.

Winter, A., Deits, R., Dorsch, D., Slocum, A., and Hosoi, A. (2014). "Razor clam to RoboClam: burrowing drag reduction mechanisms and their robotic adaptation." *Bioinspiration & biomimetics*, 9(3), 036009.

Winter, A. G., Deits, R. L. H., and Hosoi, A. E. (2012). "Localized fluidization burrowing mechanics of Ensis directus." *Journal of Experimental Biology*, 215(12), 2072-2080.